Widespread acceleration of drought propagation from the atmosphere to ecosystems in the Northern Hemisphere under climate warming

Yifei Li[1], Shengzhi Huang[1]*, Xing Yuan[2], Chong-Yu Xu[3], Jianfeng Li[4], Guoyong Leng[5], Hao Wang[6], Yi Guo[1], Wenwen Guo[1], Pei Li[1], Xudong Zheng[1], Jian Peng[7]

1 State Key Laboratory of Eco-hydraulics in Northwest Arid Region of China, Xi'an University of Technology, Xi'an 710048, China

2 School of Hydrology and Water Resources, Nanjing University of Information Science and Technology, Nanjing 210044, Jiangsu, China.

3 Department of Geosciences, University of Oslo, 0316 Oslo, Norway

4 Department of Geography and Resource Management, The Chinese University of Hong Kong, Hong Kong, China

5 Key Laboratory of Water Cycle and Related Land Surface Processes, Institute of Geographic Sciences and Natural Resources Research, Chinese Academy of Sciences, Beijing 100101, China

6 State Key Laboratory of Simulation and Regulation of Water Cycle in River Basin, China Institute of Water Resources and Hydropower Research, Beijing 100038, China

7 Department of Remote Sensing, Helmholtz Centre for Environmental Research−UFZ, Permoserstrasse 15, 04318 Leipzig, Germany

*Corresponding Author: Shengzhi Huang, huangshengzhi7788@126.com

Abstract

It remains an open question of whether the propagation from meteorological to ecological drought is accelerating under the intensifying hydrological cycle associated with global warming. Here, we investigate changes in drought propagation processes and the corresponding driving mechanisms during summer season for the Northern Hemisphere ecosystems (NHE) using multiple vegetation satellite remote sensing datasets from 1982 to 2015. The results reveal a distinct spatial pattern of decreasing drought propagation time (PT) from north to south, predominantly controlled by radiation, soil moisture, and vegetation types. Temporally, over the last three decades, the average PT in the NHE has significantly decreased by 2.64, 1.69, and 1.43 weeks under moderate, severe, and extreme drought scenarios, respectively. Approximately 60% of the NHE exhibit accelerating propagation, particularly in cropland and shrub located in the central-western United States, southwestern and eastern Europe, and the northeastern China, implying declining mean resistance of the ecosystems in these areas to drought. The accelerating drought propagation is mainly induced by warming, followed by an increase in radiation and a declining soil moisture. The observed accelerating drought propagation from the atmosphere to ecosystem highlights the necessity of effective actions to improve climate change resilience of the NHE.

Keywords: drought propagation; propagation time; meteorological drought; ecological drought; climate change; Northern Hemisphere ecosystems

1 Introduction

Water is a crucial component for plant photosynthesis and nutrient transport (Choat et al., 2018; McDowell et al., 2022). The scarcity of water available to vegetation directly affects its growth status,

thereby influencing the functionality and health of the entire ecosystem (Gampe et al., 2021; Vicente-Serrano et al., 2020). However, recent studies have shown that with the intensification of global warming, vegetation is increasingly subjected to severe water scarcity stress, and drought is gradually becoming the most critical factor limiting the stability and health of terrestrial ecosystems (Gampe et al., 2021; Jiao et al., 2021; Li et al., 2022; Yuan et al., 2019). Drought is typically triggered by precipitation deficits and gradually propagates to the soil (Entekhabi, 2023; Zhang et al., 2022). When the accumulated water deficit in the soil exceeds a certain threshold, it starts exerting pressure on the physiological processes of vegetation, leading to wilting or even death, ultimately resulting in ecological drought (Entekhabi, 2023; Jiang et al., 2021; Sadiqi et al., 2022). The propagation speed of drought signals from the atmosphere to vegetation can, to some extent, reflect the resilience of an ecosystem to maintain its stability and withstand adverse disturbances (Wu et al., 2023). Thus, accurately capturing the drought propagation time (PT) from the onset of meteorological drought to the initiation of vegetation damage is crucial for precise prediction and evaluation of the impacts of ecological drought (Fang et al., 2019; Xu et al., 2023).

Presently, drought propagation has emerged as a research hotspot, but it predominantly focuses on the propagation of drought within the atmosphere and hydrosphere, with limited attention given to terrestrial ecosystems (Entekhabi, 2023; Han et al., 2021; Slette et al., 2019; Zhang et al., 2022). However, the process of vegetation experiencing water scarcity stress is actually an overflow of drought propagation within the hydrosphere (Entekhabi, 2023; Wang et al., 2023). Despite some regional studies conducted in this field (Wang et al., 2023; Xu et al., 2023; Zhao et al., 2020), the spatial patterns of drought propagation across large spatial scales encompassing diverse ecosystems and climatic regions remain undisclosed. Furthermore, previous research has primarily characterized

the key feature of PT in drought propagation by calculating lagged cross-correlations between vegetation and drought indices (Wei et al., 2022; Xu et al., 2023; Zhao et al., 2020). This method is, however, not ideal to reflect the propagation processes under different levels of drought scenarios. In addition, the complex propagation processes are simultaneously influenced by multiple factors (Li et al., 2022; McDowell et al., 2022; Yuan et al., 2019). For instance, soil moisture, which is closely linked to vegetation water supply, can buffer meteorological drought and diminish propagation risk due to their long-term spatial distribution characteristics in a specific region (Li et al., 2022; Wu et al., 2021). Conversely, factors related to vegetation stomatal regulation and transpiration, such as vapor pressure deficit and potential evapotranspiration, may accelerate drought propagation by augmenting water consumption (Fu et al., 2022; Xi and Yuan, 2023; Yuan et al., 2019; Zhang et al., 2023). Moreover, energy-related factors such as temperature and solar radiation, as well as intrinsic characteristics of vegetation in different climatic environments, human irrigation activities, and changes in carbon dioxide concentration, can also affect the processes of drought propagation (Gampe et al., 2021; McDowell et al., 2008). However, there is a dearth of systematic studies that comprehensively investigate the specific roles of these factors in drought propagation processes and their impact on the spatial distribution pattern of drought PT. Furthermore, given the intensification of global warming and terrestrial hydrological cycle (Wang et al., 2023; Yuan et al., 2023; Zhang et al., 2022), it still remains uncertain whether the fluctuations in these influencing factors alter drought propagation processes and their potential driving mechanisms.

In this study, we will primarily focus on investigating the propagation processes from meteorological to ecological drought during the peak summer period of vigorous plant growth in the Northern Hemisphere terrestrial ecosystems (NHE, north of 30°N), which has experienced significant

warming in recent decades (Buermann et al., 2018; Vicente-Serrano et al., 2020). Here, we utilized long-term meteorological data (1982-2015) to construct the Standardized Precipitation Evapotranspiration Index (SPEI) as a measure of meteorological drought (Vicente-Serrano et al., 2013). Ecological drought was characterized using multiple sets of vegetation indices based on remote sensing observations including Normalized Difference Vegetation Index (NDVI), Leaf Area Index (LAI), and Gross Primary Productivity (GPP). Subsequently, the propagation probabilities (PP) of ecological drought caused by different levels of meteorological drought were quantified based on Copula functions and conditional probabilities. Finally, the PT under multiple drought scenarios was further identified using the PP matrix (see Methods).

Through this study, we aim to address the following questions: (1) What are the spatial distribution patterns of drought PT in the NHE across various vegetation types under different levels of drought severity? (2) Has there been a modification in the propagation process from meteorological to ecological drought under climate change, and what are the fundamental driving mechanisms behind this alteration? Moreover, for the second scientific question, we have formulated a plausible hypothesis based on existing research: owing to the influence of warming and intensified hydrological cycles, it is hypothesized that the propagation process from meteorological to ecological drought will demonstrate a notable acceleration trend across diverse vegetation ecosystems within the NHE. In the subsequent sections, we evaluate this hypothesis to answer the aforementioned question.

2 Materials and Methods

2.1 Data sources

The vegetation satellite observation data was obtained from the third-generation biweekly

Advanced Very High-Resolution Radiometer (AVHRR) NDVI (GIMMS-NDVI3g, https://ecocast.arc.nasa.gov/data/pub/gimms/3g.v0). This data a has spatial resolution of 0.083°×0.083°, and we extracted the NDVI for the summer months (June to August) from 1982 to 2015 on the NHE to investigate the vegetation response to drought. Additionally, to further ensure the robustness of the research findings, we also validated the results using satellite-based Gross Primary Productivity (GPP-GLASS) and Leaf Area Index (LAI-GLASS). These data, with a spatial resolution of 0.05°×0.05° and 8 days interval from 1982 to 2015, were obtained from the National Earth System Science Data Center, National Science & Technology Infrastructure of China (http://www.geodata.cn). The Standardized Precipitation Evapotranspiration Index (SPEI) was used to characterize meteorological drought. This index was obtained by fitting and standardizing the difference between precipitation and potential evapotranspiration. The daily precipitation from 1982 to 2015, with a spatial resolution of 0.25°×0.25°, as well as the meteorological data (temperature, pressure, solar radiation, wind speed, and relative humidity) required for calculating potential evapotranspiration (Penman-Monteith method), were provided by the global meteorological forcing dataset from Princeton University (https://hydrology.soton.ac.uk/data/pgf/v3/0.25deg/daily). To facilitate the matching of vegetation status with meteorological drought, we standardized NDVI using the SPEI calculation method, resulting in the Standardized NDVI (SNDVI), which was used to characterize ecological drought. The specific calculation procedures for SPEI and SNDVI can be found in Supplementary **Text S1**. The monthly soil moisture data used for attribution analysis (root zone soil moisture, with a depth of 1 meter and a resolution of 0.25° × 0.25°) was available from the NASN Global Land Data Assimilation System (GLDAS version 2.0 and 2.1, https://disc.gsfc.nasa.gov/datasets/?keywords=GLDAS). VPD (Vapor Pressure Deficit) and AI

(Aridity Index) were estimated using meteorological data provided by Princeton University (Yuan et al., 2019; Zomer et al., 2022). We processed and integrated the aforementioned vegetation, meteorological, and soil moisture data to a unified spatial resolution of 0.5°×0.5°. In addition, the five primary vegetation types (tundra, grassland, forest, shrubland, and cropland) in the NHE were extracted based on the GLC 2000 global vegetation map dataset (https://forobs.jrc.ec.europa.eu/products/glc2000). In this study, we classified evergreen broad-leaved and coniferous forests, deciduous broad-leaved and coniferous forests, and mixed forests into forest classification. Irrigation area data was obtained from the Global Irrigation Area Map (version 5.0) provided by the Food and Agriculture Organization of the United Nations (FAO) (https://www.fao.org/aquastat/en/geospatial-information/global-maps-irrigated-areas/latest-version).

2.2 Calculation framework for drought propagation time

The basic principle of calculating the PT from meteorological to ecological drought in this study can be summarized as follows: firstly, based on the natural dependence between vegetation and moisture content, the Copula function is employed to construct the joint distribution function between them. Then, the probability of vegetation loss under different drought scenarios and durations is calculated using the Bayesian conditional probability formula. Finally, the probability threshold interval is set and the corresponding drought duration when the threshold is first reached is selected as the optimal drought PT. The specific calculation process of PT is shown below:

The first step is to determine water-limited areas. In some regions of the NHE, vegetation is in an energy-limited state, such as extremely humid areas and high latitude cold regions (Jiao et al., 2021). Due to relatively abundant water resources in these areas, solar radiation and temperature become the primary limiting factors for vegetation growth (Lai et al., 2011). Conversely, excessive

precipitation can have an impact on photosynthesis in vegetation and may also result in waterlogging. Therefore, in this study, the Pearson correlation coefficient between summer vegetation index and multi-scale SPEI is calculated to identify water-limited regions and select them as specific study areas. The procedures are as follows:

$$r_i = correlation\left(SPEI_i, NDVI\right) \tag{1}$$

where r_i represents the Pearson correlation coefficient between summer NDVI and multi-scale SPEI, i denotes the temporal accumulation scale of SPEI. Considering the lag effect of vegetation response to the changes in environmental water, we calculated the correlation coefficients between summer NDVI and $SPEI_{1\text{-}48}$ at temporal scales ranging from 1 to 48 weeks (**Figure. S1**). If any of these correlation coefficients are positive, the corresponding grid is classified as a water-limited region.

The second step is to establish the dependence structure between summer vegetation and drought index. Multivariate joint distribution is the key to building the dependence structure between variables. In this study, Copula functions are utilized to construct a joint distribution between SNDVI and multi-scale SPEI. The core calculation formula is as follows:

$$\begin{aligned} F_{SNDVI_j, SPEI_{ij}}\left(sndvi, spei\right) &= P\left(SNDVI_j < sndvi, SPEI_{ij} < spei\right) \\ &= C\left(F_{SNDVI_j}\left(sndvi\right), F_{SPEI_{ij}}\left(spei\right)\right) \end{aligned} \tag{2}$$

where i denotes the scale of SPEI, ranging from 1 to 48 weeks, and j denotes the summer months (from June to August). $F_{SNDVI_j}\left(sndvi\right)$ and $F_{SPEI_{ij}}\left(spei\right)$ are the normal marginal distribution functions of SNDVI and SPEI, respectively, and C is the Copula function. $F_{SNDVI_j, SPEI_{ij}}$ represents the joint distribution function of the vegetation status in j month and the SPEI sequence with a time accumulation of i weeks. In this study, a total of five commonly used Copula functions were selected

171 to fit the relationship between SPEI and SNDVI. For more information about Copula functions, can
172 refer to the Supplementary **Text S2**.

173 The third step is to calculate the probability of drought propagation. Based on the joint
174 distribution of vegetation and multi-scale SPEI established in the previous step, the probability matrix
175 of drought propagation from meteorological drought to ecological drought is calculated using the
176 conditional probability formula. The specific process is illustrated in **Figure. S2**, where the green
177 rectangular blocks in the figure represent the vegetation status for each month of summer, the orange
178 blocks above represent the SPEI. Taking advantage of the multi-scale characteristics of the SPEI, we
179 calculate the probabilities of vegetation damage occurring during the 1 to 48 weeks range prior to
180 each summer month, under moderate, severe, and extreme drought scenarios. The formula for
181 propagation probability (PP) is as follows:

$$
\begin{aligned}
PP_{ij} &= P\left(SNDVI_j < -0.5 \mid x_1 < SPEI_{ij} < x_2\right) \\
&= \frac{P\left(SNDVI_j < -0.5, x_1 < SPEI_{ij} < x_2\right)}{P\left(x_1 < SPEI_{ij} < x_2\right)} \\
&= \frac{P\left(SNDVI_j < -0.5, SPEI_{ij} < x_2\right) - P\left(SNDVI_j < -0.5, SPEI_{ij} < x_1\right)}{P\left(SPEI_{ij} < x_2\right) - P\left(SPEI_{ij} < x_1\right)} \\
&= \frac{C\left(F_{SNDVI_j}(-0.5), F_{SPEI_{ij}}(x_2)\right) - C\left(F_{SNDVI_j}(-0.5), F_{SPEI_{ij}}(x_1)\right)}{F_{SPEI_{ij}}(x_2) - F_{SPEI_{ij}}(x_1)}
\end{aligned}
\tag{3}
$$

183 where PP_{ij} represents the probability values of drought propagation at *i*-weeks scale for the month of
184 *j*. The interval ($x_1 < SPEI_{ij} < x_2$) represents the intensity of meteorological drought. When it takes
185 the values (-1, -1.5) and (-1.5, -2), they respectively represent moderate and severe drought scenarios.
186 In addition, setting *SNDVI*<-0.5 indicates that vegetation begins to exhibit adverse responses to the
187 meteorological drought, indicating the occurrence of ecological drought. Furthermore, when
188 meteorological drought is in an extreme scenario, the above equation can be simplified as follows:

$$PP_{ij} = P\left(SNDVI_j < -0.5 \mid SPEI_{ij} < -2\right) = \frac{P\left(SNDVI_j < -0.5, SPEI_{ij} < -2\right)}{P\left(SPEI_{ij} - 2\right)} = \frac{C\left(F_{SNDVI_j}\left(-0.5\right), F_{SPEI_{ij}}\left(-2\right)\right)}{F_{SPEI_{ij}}\left(-2\right)} \quad (4)$$

The final step is to extract the drought PT. Based on the PP from the previous step, we set specific probability thresholds to extract the drought PT. Taking an arbitrary grid cell within the study area as an example, the specific procedure is as follows: starting from the moderate drought scenario, we set the probability threshold interval for extracting the drought PT as [0.5, 0.7]. Initially, using a threshold value of 0.7, we start from the bottom of the probability matrix (**Figure. S2**) and iterate through each drought duration *i* from 1 to 48, checking if PP_{ij} is equal to or exceeds 0.7. The corresponding value of *i*, when it first meets the threshold requirement, represents the PT from meteorological to ecological drought for that grid cell under the scenario of moderate drought. If after examining all drought duration scales, none of them reach a propagation probability of 0.7, we decrease the probability threshold requirement by -0.1 steps and repeat the aforementioned procedure to extract the PT. Eventually, if the extraction threshold is reduced to 0.5 and the probability matrix still fails to meet the extraction requirement, the grid cell is discarded, indicating that the grid cannot trigger vegetation loss under the moderate meteorological drought. In the severe drought scenario, if the grid cell has a PT under the moderate drought, we use the corresponding extraction probability of PT under the moderate drought scenario as the threshold to iteratively check the probability matrix and extract the PT under the severe drought scenario. However, if the grid cannot trigger vegetation loss under the moderate drought conditions, then the extraction of PT under the severe drought is still performed using the probability threshold range of [0.5, 0.7]. The extraction of PT under the extreme drought scenario follows the same procedure as under the severe drought. By following the above procedure,

we can ensure that as the drought scenario becomes more severe, the corresponding propagation probabilities of PT are larger, thereby increasing the credibility.

2.3 Attribution analysis

In this study, we primarily employed partial dependence plots based on the Random Forest model to analyze the spatial distribution patterns of drought PT and the driving mechanisms behind its changes. In analyzing the variables contributing to the spatial distribution patterns of PT, we included the PT of all grid cells in the study area as the response variable. The influencing variables including long-term average values of summer Rn, SM, Pre, Ta, AI, and VPD, were used as explanatory variables. The regression Random Forest model employed consisted of 500 decision trees, with each tree split using the CART method and the minimum terminal node size set at 5. The permutation method was employed in this research to score and rank the explanatory variables that affect the distribution pattern of PT (Pham and Brabyn, 2017). This approach involved randomly permuting the correspondence between a particular explanatory variable and the response variable. Subsequently, we re-fitted the Random Forest model using the permuted variables and measured the resulting decrease in model prediction accuracy. The magnitude of the decrease in accuracy served as an indicator of the influence of the explanatory variable on the PT, with a larger decrease indicating a stronger impact and thus a higher importance score. In addition, in order to analyze the spatial distribution of PT and its independent response to each explanatory variable, we utilized partial dependence plots based on the Random Forest model to visualize the response functions of PT to each explanatory variable. Furthermore, bootstrap sampling was applied to estimate the 95% confidence intervals of the response functions (Sutton, 2005).

In attributing the dynamic changes of PT, we employed a moving window approach to segment

the original data and calculated PT for each window. The PT change series for each grid cell was treated as the response variable, the corresponding driving factors (Ta, Rn, SM, PET, VPD, and Pre) under each window were considered as explanatory variables. To facilitate comparisons of PT variations with the driving factors across different grid cells, we normalized both PT and the driving factors. Then, a Random Forest model (with the same structure as the aforementioned model) was individually built for each grid in the study area. The permutation method was also utilized to assess the dominant driving factors of PT variations under different drought scenarios for each grid, and their spatial distribution maps were generated. Lastly, by averaging the partial dependence plots of the dominant driving factors for each grid, we obtained the overall average response functions of PT to each driving factor. Additionally, bootstrap sampling was also used to calculate the 95% confidence intervals of the average response values.

3 Results and Discussion

3.1 Drought PT exhibits a decreasing spatial pattern from high to mid-latitudes.

Figure. 1(a)-(c) and **Figure. S3(a)-(c)** depict the spatial distribution patterns of drought PT and the corresponding propagation probability (PP), which indicates the likelihood of ecological drought resulting from meteorological drought, across the NHE during the summer season. The results demonstrate a clear latitudinal distribution pattern for both PT and PP. In high-latitude regions (above 60°N), the average PT is approximately 30 weeks. However, as latitude decreases from 60°N to 30°N, the PT shortens to around 10 weeks in most areas. In terms of PP, it is generally higher than 0.7 in low-latitude regions and decreases to around 0.5-0.6 as latitude increases. Additionally, with the intensification of meteorological drought levels, the PT required to trigger ecological drought significantly decreases, the corresponding PP noticeably increases, and the area of vegetation affected

by drought stress also expands. In terms of spatial distribution, lower PT values are observed in the central and western regions of the United States, southwestern Europe, the central Asia-Europe continent, and parts of East Asia. In extreme drought scenarios, the PT in these areas is around 5 weeks, while the average PP is above 0.8. In contrast, the Far East region of Russia requires a longer PT for drought to trigger vegetation damage, with PT generally around 35 weeks.

From the perspective of different vegetation types, tundra and forest ecosystems exhibit the strongest resilience to drought. These ecosystems necessitate a longer duration of water deficit accumulation to trigger ecological drought. In moderate and severe drought scenarios, the average PT is approximately above 20 weeks, and the probability of vegetation damage is relatively low, with an average PP below 0.6 (**Figure. 1(d)** and **Figure. S3(d)**). However, cropland, grassland, and shrub ecosystems exhibit weaker resistance to drought, responding quickly after the onset of meteorological drought. In extreme drought scenarios, the average PT for these ecosystems is less than 10 weeks, and the PP remains above 0.7. Furthermore, as the severity of meteorological drought increases, the PT for all vegetation types noticeably decreases, while the PP increases (**Figure. 1(d)** and **Figure. S3(d)**).

3.2 Radiation, soil moisture, and vegetation types affect the spatial pattern of drought PT

The drought propagation processes are influenced by multiple factors. In order to analyze the reasons behind the spatial distribution pattern of PT (**Figure. 1**), a Random Forest model is employed to investigate the mechanisms of the impacts of various factors on PT (see Methods). In this study, we select seven major variables closely related to vegetation growth for analysis: solar radiation (Rn), soil moisture (SM), precipitation (Pre), air temperature (Ta), aridity index (AI), vapor pressure deficit (VPD) and potential evapotranspiration (PET) (Flo et al., 2022; Fu et al., 2022; Li et al., 2023). **Figure.**

2 displays the relative importance scores of different variables in influencing the spatial distribution of drought PT. It can be observed that energy variables (Rn, Ta) and water supply variables (SM, Pre) are the two most crucial factors constraining the propagation speed of meteorological drought to vegetation. Water and energy are essential elements for vegetation to undergo photosynthesis (McDowell et al., 2022), and therefore they have a significant impact on vegetation's resilience to cope with drought (Schwalm et al., 2017).

To further elucidate the mechanisms by which different variables affect the PT, taking extreme meteorological drought scenarios as an example, we employ Partial Dependence Plot (PDP) base on the Random Forest model to generate response functions for the top six influential variables (**Figure. 3**). Each influencing variable is analyzed individually. First, regarding Rn, PT remains at a high level with no significant change when Rn is within a lower range. However, once Rn surpasses 1400 MJ/m^2, PT displays a clear declining trend (**Figure. 3(a)**). The response of drought PT to Rn may be related to the spatial distribution of Rn in the NHE. As shown in **Figure. S4(a)**, the regions where summer Rn is below 1400 MJ/m^2 are predominantly situated north of 60°N. Higher Rn during the summer in these regions can potentially facilitate the melting of snow and frozen soil, thereby replenishing soil moisture and creating a more favorable environment for vegetation survival (Li et al., 2021; Liu et al., 2022). Hence, in regions with lower Rn values, the drought PT is longer and less sensitive to the variations of Rn. In contrast, regions with Rn higher than 1400 MJ/m^2 are primarily situated between 30°-60°N, which has a large proportion of arid and semi-arid areas (Gampe et al., 2021). The higher Rn in these regions promotes soil moisture evaporation, that can accelerate the drought propagation processes (Heck et al., 2020). The response of PT to SM generally exhibits a synchronous upward trend (**Figure. 3(b)**), implying that in regions with higher soil moisture content, vegetation exhibits a

longer drought PT (**Figure. 1** and **Figure. S4(b)**). As SM serves as the main water source for most vegetation (Green et al., 2019), higher levels of SM content are inclined to alleviate and delay the stress exerted by meteorological drought on vegetation (Li et al., 2022; Stocker et al., 2018). The impact of Pre on PT differs from that of SM. PT exhibits a two-stage pattern with an initial decrease followed by an increase as Pre increases (**Figure. 3(c)**). The first stage of PT response to Pre may be influenced by the interference of longer drought PT in high-latitude regions despite lower precipitation amounts. The subsequent stage indicates that in mid-latitude regions, vegetation exhibits a stronger resilience to resist drought as Pre increases. Furthermore, PT shows an overall decreasing trend with increasing Ta and VPD (**Figure. 3(d) and (f)**). When experiencing meteorological drought, higher Ta tends to accelerate soil moisture depletion (Samaniego et al., 2018). Simultaneously, higher VPD can impact vegetation photosynthesis by stimulating stomatal closure (Grossiord et al., 2020). Thus, both factors contribute to an acceleration of unfavorable vegetation responses to the meteorological drought (Fu et al., 2022; Gampe et al., 2021; McDowell et al., 2022). Finally, for the AI, it can be observed that as its value increases gradually (higher AI meaning wetter conditions), PT also shows an increasing trend (**Figure. 3(e)**). This indicates that vegetation in arid and semi-arid regions responds to drought more quickly than in humid areas.

Apart from being influenced by the mentioned natural environmental variables, the strategies adopted by different vegetation types to cope with water deficiency can also impact the drought propagation processes (Konings et al., 2017; McDowell et al., 2008). For instance, forest ecosystems can alleviate the impacts of meteorological drought by accessing groundwater from deeper layers through their well-developed root systems (Choat et al., 2018; Mackay et al., 2020; McDowell et al., 2019). This reduces their vulnerability to drought and allows them to have a longer PT (**Figure. 1(d)**).

However, for most grassland and shrub ecosystems located at mid-latitude regions, their roots mainly consist of dispersed lateral or shallow roots rather than the dominant taproot found in woody plants (Konings et al., 2017). Consequently, these plants are unable to fully exploit underground water, which significantly increases the probability of rapid wilting or even death during extreme meteorological drought (Sippel et al., 2018). Nevertheless, these plant species have evolved shorter seed maturation periods, providing them with faster recovery capabilities (Yang Li et al., 2023; Schwalm et al., 2017). Cropland ecosystems, face similar conditions to grassland and shrub during the drought periods. However, irrigation activities may alleviate the adverse effects of water scarcity (McDermid et al., 2023), leading to lower drought propagation probabilities and slightly longer PT. Lastly, in high-latitude tundra ecosystems, elevated temperatures and intensified radiation often coincide with a certain degree of drought (Sungmin et al., 2022). This may accelerate the thawing of solid-state moisture, mitigating soil water deficit, and maintaining suitable growth temperatures (Hu et al., 2022), resulting in a longer drought PT. In summary, the spatial distribution patterns of drought PT in the NHE are shaped by the intricate interplay between natural conditions and the long-term evolution of various vegetation strategies for drought resistance.

3.3 Widespread acceleration of propagation from meteorological to ecological drought over the last three decades

In order to explore the dynamic changes in the drought propagation processes in the context of climate change over the last three decades (1982-2015). We utilized a moving window approach with a window length of 15 years to determine the drought PT for each window. Then the Mann-Kendall (MK) test was employed to analyze the significance of the observed trends (see **Methods**). **Figure. 4(a)** displays the overall trend in the average PT of all grid cells in NHE under different drought

341 scenarios. The results generally support our hypothesis that reveals a widespread acceleration in the
342 propagation from meteorological to ecological drought within the NHE. Specifically, by estimating
343 the decrease slope from **Figure. 4(a)**, over the last three decades, under the moderate, severe, and
344 extreme drought scenarios, the average PT in the NHE significantly decreased by 2.64, 1.69, and 1.43
345 weeks ($p<0.01$), respectively. **Figure. 5** depicts the spatial patterns of PT changes under the three
346 drought scenarios. It can be observed that a majority of the NHE regions show a shortening trend in
347 the drought PT over the last three decades. In the moderate, severe, and extreme drought scenarios,
348 the proportion of areas exhibiting a shortening trend in drought PT reaches 58%, 56%, and 57%,
349 respectively. Moreover, among these areas, the proportion with a significant decrease in drought PT
350 is 29%, 28%, and 27% respectively ($p<0.01$). The proportion of grid cells with an increasing trend in
351 PT is 42%, 44%, and 43% under the three drought scenarios, respectively. However, the proportion
352 with a significant increase does not exceed 17% ($p<0.01$) in all of the drought scenarios. In addition,
353 the areas exhibiting a significant shortening trend in drought PT are spatially concentrated. Regions
354 including the cropland and shrub ecosystems in the central-western of the United States, cropland
355 ecosystems in southwestern Europe (including the Iberian Peninsula and southwestern France),
356 cropland and grassland ecosystems in eastern Europe (Ukraine and southwestern Russia), as well as
357 grassland and cropland ecosystems in central Asia and northeastern China, demonstrate a significant
358 trend of shortened drought PT ($p<0.01$). In contrast, the grid cells with a significant increase in PT
359 are relatively scattered. For instance, regions such as southwestern United Kingdom, central Europe,
360 and certain areas of central Eurasia demonstrate a significant increase trend in the drought PT ($p<0.01$)
361 (**Figure. 5**). Our analyses in Supplementary **Text S3** with different choices of window length (from
362 17 to 19 years) and vegetation index (GPP and LAI) show the robustness of the results

3.4 Warming, increased radiation, and decreased soil moisture accelerate drought propagation

To analyze the reasons and driving mechanisms for the changes in drought PT over the last three decades, we have also employed the Random Forest model to conduct a gridded attribution analysis on various driving factors (including Pre, Ta, Rn, SM, PET, VPD, and AI) that influence the drought propagation processes. **Figure. 6** displays the spatial distribution of the dominant driving variables that influence changes in the drought PT under different drought scenarios. We found that Ta, Rn, and SM are the main driving variables affecting the changes of drought PT. The combined impact area of these three factors exceeds 50% of the total study area under all three drought scenarios. Other factors such as PET, VPD, and Pre have dominant influence areas on the changes of PT ranging from 10% to 15%. The AI has the smallest area proportion and does not exceed 10% under any of the three drought scenarios.

In the context of climate change, how do fluctuations in these factors drive the changes of PT? To investigate this, we have separately plotted the response functions of PT to each driving variables over the last three decades (**Figure. 4(b)**). It can be observed that factors related to energy and water consumption, such as Ta, Rn, PET and VPD, are negatively correlated with PT changes under all three drought scenarios. It means that an increase in these variables drives a reduction change in drought PT. This finding is consistent with our understanding of the response mechanism of vegetation to water scarcity. In the initial stages of meteorological drought, the pre-existing SM can provide water for vegetation, thus alleviating the adverse impacts caused by drought (Li et al., 2023). However, as the drought persists, the increase in Ta and Rn caused by climate change will intensify the evaporation of SM (Konapala et al., 2020). As the primary source of water for plants, the decrease in SM further restricts the water uptake capacity of plant roots (Choat et al., 2018; Zhang et al., 2023).

As vegetation water deficit accumulates to a certain threshold, it may trigger embolism in the plant's xylem vessels, hindering the transport of water and nutrients within the plant and ultimately leading to irreversible hydraulic failure (Choat et al., 2018; Gampe et al., 2021; McDowell et al., 2022). On the other hand, an increase in VPD can stimulate plants to close or restrict stomatal conductance (Yuan et al., 2019). Despite this regulation can reduce plant transpiration and minimize water loss during drought to prevent embolism, it also diminishes the intake of carbon dioxide (McDowell et al., 2019). This limitation restricts the plant's ability to carry out photosynthesis and synthesize organic compounds (López et al., 2021). As drought persists, this can eventually lead to carbon starvation in plants (McDowell et al., 2008). Furthermore, it is worth noting that there are complex feedback mechanisms between hydraulic failure and carbon starvation, which can mutually reinforce each other and further accelerate the vegetation's response to drought (McDowell et al., 2022). On the contrary, PT shows a positive correlation with factors related to water supply (such as SM and Pre) under all three drought scenarios (**Figure. 4(b)**). This means that as SM and Pre increase, PT also exhibits a simultaneous prolongation trend. Increased Pre, especially an increase in SM, can act as a buffer against meteorological drought. Vegetation can extend its PT to meteorological drought by utilizing sufficient SM (Li et al., 2022).

To further analyze the specific reasons for the spatial distribution of the changes in drought PT across different regions in the NHE, we have also plotted the change trends of the main driving variables over the last three decades (**Figure. S5**). The significant decrease in drought PT in the central-western United States is mainly associated with the increase in Ta, Rn, and PET, as well as the decrease in SM and Pre. The significant decrease in drought PT in southwestern Europe may be attributed to the warming and reduced Pre in that region. On the other hand, eastern Europe is

primarily influenced by increases in PET and VPD, as well as a warming and a decrease in SM, which together lead to a shortened PT. The decrease PT in central Eurasia is primarily influenced by warming, VPD rise, and Rn increase. Northeastern China is mainly affected by Rn and VPD enhancement, as well as reduced Pre. It is noteworthy that in the regions where a significant reduction in drought PT was observed within the NHE, recent studies have also reported an enhanced reliance of vegetation on water availability (Jiao et al., 2021; W. Li et al., 2022; Samaniego et al., 2018; Zhang et al., 2023). This finding serves to a certain extent as validation for the reliability of our results. Furthermore, for the regions where PT exhibits a significant increase (such as central Europe and some areas in central Eurasia), it may be attributed to the influence of increased Pre or SM in these regions, as well as decreased Rn and PET.

3.5 Comparing the dynamics in drought PT among different vegetation types and irrigated/non-irrigated regions

As shown in **Figure. S5**, significant changes have been observed in the variables closely related to vegetation growth such as Ta, Rn, and SM over the last three decades in NHE. Are there consistent drought PT changes among different vegetation types and between irrigated and non-irrigated regions in the context of climate change? To answer this, we extracted grids corresponding to different vegetation types and irrigated and non-irrigated areas, and then calculated regional averages of drought PT to determine their trends under the changing environmental conditions. As shown in **Figure. 7**, among the four main vegetation types on the NHE, the acceleration of drought propagation to cropland and shrubland ecosystems is most pronounced. Taking cropland ecosystems as an example, over the last three decades, the drought PT of cropland has decreased by approximately 4.14, 3.15, and 2.47 weeks ($P<0.01$) under moderate, severe, and extreme meteorological drought

scenarios, respectively. These values are evidently higher than the overall average level of accelerated drought propagation observed on the NHE (**Figure. 4(a)**). In addition, grassland ecosystems also exhibited a decreasing trend in drought PT under the three drought scenarios. In contrast to the aforementioned vegetation types, forest ecosystems exhibited a reduction in PT only under the moderate meteorological drought, with an average decrease of approximately 1.23 weeks over the last three decades ($P<0.01$). However, there was no significant change observed under moderate and extreme drought scenarios ($P>0.05$) (**Figure. 7**).

The divergence PT changes of different ecosystems to drought may be attributed to the interplay between vegetation characteristics and external environmental factors. Firstly, from the perspective of vegetation characteristics, forest ecosystems generally exhibit higher species diversity and well-developed root systems compared to cropland, grassland, and shrub ecosystems (Gampe et al., 2021; Schwalm et al., 2017; Spohn et al., 2023). Therefore, they have inherent advantages in resisting drought and external environmental disturbances (McDowell et al., 2008). From the external environmental perspective, the mid-latitude regions where cropland, grassland, and shrub ecosystems are located experience more pronounced warming and a greater decrease in SM compared to other regions (**Figure. S5(a) and (c)**). This leads to stronger drought stress in the mid-latitude regions (Jiao et al., 2021), ultimately resulting in a larger reduction in their drought PT.

In addition, for cropland ecosystems, we also conducted comparative analysis on the differences in crop responses to drought between irrigated and non-irrigated areas. The results indicate that regions with irrigation facilities can alleviate the impact of climate change on crops. In the last three decades, irrigation has significantly improved the resilience of crops to meteorological drought, particularly in mitigating the impacts of severe and extreme drought. In these two scenarios, the

drought PT has increased by 1.56 ($P<0.01$) and 1.81 ($P<0.05$) weeks, respectively (**Figure. 8**). On the contrary, non-irrigated areas exhibit a more pronounced decrease in drought PT compared to the overall cropland ecosystem (**Figure. 8**). Although human irrigation activities can effectively mitigate the impacts of climate change on agricultural ecosystems, unfortunately, irrigated farmland only accounts for around 20% of global agriculture (McDermid et al., 2023). Our findings reveal that in major grain-producing regions worldwide, such as the central-western United States, the Ukrainian Plain, the southwestern region of Russia, and northeastern China, the drought PT in these rain-fed agricultural areas is significantly decreasing. Additionally, this finding is consistent with previous studies that have shown a severe increase in negative GPP extremes in croplands of mid-latitude regions in the NHE (Gampe et al., 2021). The accelerated propagation of meteorological drought to croplands may imply that compared to the last, a larger area of cultivated land can be affected by drought in a shorter period of time. This will have an unfavorable impact on the prevention and control of agricultural drought, and also posing a severe threat to global food security.

4 Conclusion

In this study, we firstly elucidated the spatial distribution patterns of drought propagation in NHE under different levels of meteorological drought stress. Forest and tundra ecosystems located at higher latitudes were observed to have greater resilience to meteorological drought compared to grassland, shrubland, and cropland ecosystems in mid-latitudes. The overall distribution pattern of drought PT demonstrated a decreasing trend from north to south along the latitudinal gradient. Additionally, existing research suggests that the fertilization effect stemming from increased carbon dioxide concentration has improved vegetation water use efficiency, resulting in a global greening trend (Keenan et al., 2013; Piao et al., 2020; Schimel et al., 2015). However, our investigation using

multiple sets of vegetation remote sensing data reveals that over the last three decades (1982-2015), the drought propagation from the atmosphere to ecosystem has significantly accelerated due to warming, increased radiation, and declining soil moisture levels. This finding essentially supports the hypothesis mentioned in the introduction. Specifically, ecosystems such as croplands, grasslands, and shrublands located in mid-latitudes exhibited a notable decreasing trend in drought PT under various levels of drought scenarios. This discovery indicates that the average resilience of NHE to drought is diminishing. With future warming continuing, the impact of drought on terrestrial ecosystems will likely become more rapid, potentially posing significant challenges in predicting and controlling ecological drought and wildfires. Furthermore, as a globally important carbon sink region (Buermann et al., 2018; Jiao et al., 2021; Yang Li et al., 2023), droughts in the NHE under the warming background may have a greater impact on global carbon sink fluctuations. Further investigation is warranted to evaluate the long-term sustainability of the global vegetation greening trend in light of the accelerated propagation of drought.

Declaration of competing interest

The authors declare no potential conflicts of interest with respect to the research, authorship, or publication of this article.

Acknowledgments

This research was jointly supported by the Strategic Priority Research Program of the Chinese Academy of Sciences (grant number XDA28060100), the National Natural Science Foundation of China (grant number 52279026), and the National Key Research and Development Program of China

(grant number 2021YFC3000203).

References

Buermann, W., Forkel, M., O'Sullivan, M., Sitch, S., Friedlingstein, P., Haverd, V., Jain, A.K., Kato, E., Kautz, M., Lienert, S., Lombardozzi, D., Nabel, J.E.M.S., Tian, H., Wiltshire, A.J., Zhu, D., Smith, W.K., Richardson, A.D., 2018. Widespread seasonal compensation effects of spring warming on northern plant productivity. Nature 562, 110–114. https://doi.org/10.1038/s41586-018-0555-7

Choat, B., Brodribb, T.J., Brodersen, C.R., Duursma, R.A., López, R., Medlyn, B.E., 2018. Triggers of tree mortality under drought. Nature 558, 531–539. https://doi.org/10.1038/s41586-018-0240-x

Entekhabi, D., 2023. Propagation in the Drought Cascade: Observational Analysis Over the Continental US. Water Resour. Res. 59, 1–19. https://doi.org/10.1029/2022WR032608

Fang, W., Huang, S., Huang, Q., Huang, G., Wang, H., Leng, G., Wang, L., Guo, Y., 2019. Probabilistic assessment of remote sensing-based terrestrial vegetation vulnerability to drought stress of the Loess Plateau in China. Remote Sens. Environ. 232, 111290. https://doi.org/10.1016/j.rse.2019.111290

Flo, V., Martínez-Vilalta, J., Granda, V., Mencuccini, M., Poyatos, R., 2022. Vapour pressure deficit is the main driver of tree canopy conductance across biomes. Agric. For. Meteorol. 322. https://doi.org/10.1016/j.agrformet.2022.109029

Fu, Z., Ciais, P., Prentice, I.C., Gentine, P., Makowski, D., Bastos, A., Luo, X., Green, J.K., Stoy, P.C., Yang, H., Hajima, T., 2022. Atmospheric dryness reduces photosynthesis along a large

range of soil water deficits. Nat. Commun. 13. https://doi.org/10.1038/s41467-022-28652-7

Gampe, D., Zscheischler, J., Reichstein, M., O'Sullivan, M., Smith, W.K., Sitch, S., Buermann, W., 2021. Increasing impact of warm droughts on northern ecosystem productivity over recent decades. Nat. Clim. Chang. 11, 772–779. https://doi.org/10.1038/s41558-021-01112-8

Green, J.K., Seneviratne, S.I., Berg, A.M., Findell, K.L., Hagemann, S., Lawrence, D.M., Gentine, P., 2019. Large influence of soil moisture on long-term terrestrial carbon uptake. Nature 565, 476–479. https://doi.org/10.1038/s41586-018-0848-x

Grossiord, C., Buckley, T.N., Cernusak, L.A., Novick, K.A., Poulter, B., Siegwolf, R.T.W., Sperry, J.S., McDowell, N.G., 2020. Plant responses to rising vapor pressure deficit. New Phytol. 226, 1550–1566. https://doi.org/10.1111/nph.16485

Han, Z., Huang, S., Huang, Q., Leng, G., Liu, Y., Bai, Q., He, P., Liang, H., Shi, W., 2021. GRACE-based high-resolution propagation threshold from meteorological to groundwater drought. Agric. For. Meteorol. 307, 108476. https://doi.org/10.1016/j.agrformet.2021.108476

Heck, K., Coltman, E., Schneider, J., Helmig, R., 2020. Influence of Radiation on Evaporation Rates: A Numerical Analysis. Water Resour. Res. 56. https://doi.org/10.1029/2020WR027332

Hu, G., Zhao, L., Wu, T., Wu, X., Park, H., Li, R., Zhu, X., Ni, J., Zou, D., Hao, J., Li, W., 2022. Continued Warming of the Permafrost Regions Over the Northern Hemisphere Under Future Climate Change. Earth's Futur. 10, 1–21. https://doi.org/10.1029/2022EF002835

Jiang, T., Su, X., Singh, V.P., Zhang, G., 2021. A novel index for ecological drought monitoring based on ecological water deficit. Ecol. Indic. 129, 107804. https://doi.org/10.1016/j.ecolind.2021.107804

536 Jiao, W., Wang, L., Smith, W.K., Chang, Q., Wang, H., D'Odorico, P., 2021. Observed increasing
537 water constraint on vegetation growth over the last three decades. Nat. Commun. 12, 1–9.
538 https://doi.org/10.1038/s41467-021-24016-9

539 Keenan, T.F., Hollinger, D.Y., Bohrer, G., Dragoni, D., Munger, J.W., Schmid, H.P., Richardson,
540 A.D., 2013. Increase in forest water-use efficiency as atmospheric carbon dioxide concentrations
541 rise. Nature 499, 324–327. https://doi.org/10.1038/nature12291

542 Konapala, G., Mishra, A.K., Wada, Y., Mann, M.E., 2020. Climate change will affect global water
543 availability through compounding changes in seasonal precipitation and evaporation. Nat.
544 Commun. 11. https://doi.org/10.1038/s41467-020-16757-w

545 Konings, A.G., Williams, A.P., Gentine, P., 2017. Sensitivity of grassland productivity to aridity
546 controlled by stomatal and xylem regulation. Nat. Geosci. 10, 284–288.
547 https://doi.org/10.1038/ngeo2903

548 Lai, W.L., Wang, S.Q., Peng, C.L., Chen, Z.H., 2011. Root features related to plant growth and
549 nutrient removal of 35 wetland plants. Water Res. 45, 3941–3950.
550 https://doi.org/10.1016/j.watres.2011.05.002

551 Li, T., Chen, Y.Z., Han, L.J., Cheng, L.H., Lv, Y.H., Fu, B.J., Feng, X.M., Wu, X., 2021. Shortened
552 duration and reduced area of frozen soil in the Northern Hemisphere. Innovation 2.
553 https://doi.org/10.1016/j.xinn.2021.100146

554 Li, W., Migliavacca, M., Forkel, M., Denissen, J.M.C., Reichstein, M., Yang, H., Duveiller, G.,
555 Weber, U., Orth, R., 2022. Widespread increasing vegetation sensitivity to soil moisture. Nat.
556 Commun. 13, 1–9. https://doi.org/10.1038/s41467-022-31667-9

557 Li, Yifei, Huang, S., Wang, H., Huang, Q., Li, P., Zheng, X., Wang, Z., Jiang, S., Leng, G., Li, J.,
558 Peng, J., 2023. Warming and greening exacerbate the propagation risk from meteorological to
559 soil moisture drought. J. Hydrol. 622. https://doi.org/10.1016/j.jhydrol.2023.129716

560 Li, Y., Huang, S., Wang, H., Zheng, X., Huang, Q., Deng, M., Peng, J., 2022. High-resolution
561 propagation time from meteorological to agricultural drought at multiple levels and
562 spatiotemporal scales. Agric. Water Manag. 262, 107428.
563 https://doi.org/10.1016/j.agwat.2021.107428

564 Li, Yang, Zhang, W., Schwalm, C.R., Gentine, P., Smith, W.K., Ciais, P., Kimball, J.S., Gazol, A.,
565 Kannenberg, S.A., Chen, A., Piao, S., Liu, H., Chen, D., Wu, X., 2023. Widespread spring
566 phenology effects on drought recovery of Northern Hemisphere ecosystems. Nat. Clim. Chang.
567 13, 182–188. https://doi.org/10.1038/s41558-022-01584-2

568 Liu, Z., Kimball, J.S., Ballantyne, A.P., Parazoo, N.C., Wang, W.J., Bastos, A., Madani, N., Natali,
569 S.M., Watts, J.D., Rogers, B.M., Ciais, P., Yu, K., Virkkala, A.M., Chevallier, F., Peters, W.,
570 Patra, P.K., Chandra, N., 2022. Respiratory loss during late-growing season determines the net
571 carbon dioxide sink in northern permafrost regions. Nat. Commun. 13.
572 https://doi.org/10.1038/s41467-022-33293-x

573 López, J., Way, D.A., Sadok, W., 2021. Systemic effects of rising atmospheric vapor pressure deficit
574 on plant physiology and productivity. Glob. Chang. Biol. 27, 1704–1720.
575 https://doi.org/10.1111/gcb.15548

576 Mackay, D.S., Savoy, P.R., Grossiord, C., Tai, X., Pleban, J.R., Wang, D.R., McDowell, N.G., Adams,
577 H.D., Sperry, J.S., 2020. Conifers depend on established roots during drought: results from a

coupled model of carbon allocation and hydraulics. New Phytol. 225, 679–692. https://doi.org/10.1111/nph.16043

McDermid, S., Nocco, M., Lawston-Parker, P., Keune, J., Pokhrel, Y., Jain, M., Jägermeyr, J., Brocca, L., Massari, C., Jones, A.D., Vahmani, P., Thiery, W., Yao, Y., Bell, A., Chen, L., Dorigo, W., Hanasaki, N., Jasechko, S., Lo, M.H., Mahmood, R., Mishra, V., Mueller, N.D., Niyogi, D., Rabin, S.S., Sloat, L., Wada, Y., Zappa, L., Chen, F., Cook, B.I., Kim, H., Lombardozzi, D., Polcher, J., Ryu, D., Santanello, J., Satoh, Y., Seneviratne, S., Singh, D., Yokohata, T., 2023. Irrigation in the Earth system. Nat. Rev. Earth Environ. 4, 435–453. https://doi.org/10.1038/s43017-023-00438-5

McDowell, N., Pockman, W.T., Allen, C.D., Breshears, D.D., Cobb, N., Kolb, T., Plaut, J., Sperry, J., West, A., Williams, D.G., Yepez, E.A., 2008. Mechanisms of plant survival and mortality during drought: Why do some plants survive while others succumb to drought? New Phytol. 178, 719–739. https://doi.org/10.1111/j.1469-8137.2008.02436.x

McDowell, N.G., Grossiord, C., Adams, H.D., Pinzón-Navarro, S., Mackay, D.S., Breshears, D.D., Allen, C.D., Borrego, I., Dickman, L.T., Collins, A., Gaylord, M., McBranch, N., Pockman, W.T., Vilagrosa, A., Aukema, B., Goodsman, D., Xu, C., 2019. Mechanisms of a coniferous woodland persistence under drought and heat. Environ. Res. Lett. 14. https://doi.org/10.1088/1748-9326/ab0921

McDowell, N.G., Sapes, G., Pivovaroff, A., Adams, H.D., Allen, C.D., Anderegg, W.R.L., Arend, M., Breshears, D.D., Brodribb, T., Choat, B., Cochard, H., De Cáceres, M., De Kauwe, M.G., Grossiord, C., Hammond, W.M., Hartmann, H., Hoch, G., Kahmen, A., Klein, T., Mackay, D.S.,

Mantova, M., Martínez-Vilalta, J., Medlyn, B.E., Mencuccini, M., Nardini, A., Oliveira, R.S., Sala, A., Tissue, D.T., Torres-Ruiz, J.M., Trowbridge, A.M., Trugman, A.T., Wiley, E., Xu, C., 2022. Mechanisms of woody-plant mortality under rising drought, CO2 and vapour pressure deficit. Nat. Rev. Earth Environ. 3, 294–308. https://doi.org/10.1038/s43017-022-00272-1

Pham, L.T.H., Brabyn, L., 2017. Monitoring mangrove biomass change in Vietnam using SPOT images and an object-based approach combined with machine learning algorithms. ISPRS J. Photogramm. Remote Sens. 128, 86–97. https://doi.org/10.1016/j.isprsjprs.2017.03.013

Piao, S., Wang, X., Park, T., Chen, C., Lian, X., He, Y., Bjerke, J.W., Chen, A., Ciais, P., Tømmervik, H., Nemani, R.R., Myneni, R.B., 2020. Characteristics, drivers and feedbacks of global greening. Nat. Rev. Earth Environ. 1, 14–27. https://doi.org/10.1038/s43017-019-0001-x

Sadiqi, S.S.J., Hong, E.M., Nam, W.H., Kim, T., 2022. Review: An integrated framework for understanding ecological drought and drought resistance. Sci. Total Environ. 846, 157477. https://doi.org/10.1016/j.scitotenv.2022.157477

Samaniego, L., Thober, S., Kumar, R., Wanders, N., Rakovec, O., Pan, M., Zink, M., Sheffield, J., Wood, E.F., Marx, A., 2018. Anthropogenic warming exacerbates European soil moisture droughts. Nat. Clim. Chang. 8, 421–426. https://doi.org/10.1038/s41558-018-0138-5

Schimel, D., Stephens, B.B., Fisher, J.B., 2015. Effect of increasing CO2 on the terrestrial carbon cycle. Proc. Natl. Acad. Sci. U. S. A. 112, 436–441. https://doi.org/10.1073/pnas.1407302112

Schwalm, C.R., Anderegg, W.R.L., Michalak, A.M., Fisher, J.B., Biondi, F., Koch, G., Litvak, M., Ogle, K., Shaw, J.D., Wolf, A., Huntzinger, D.N., Schaefer, K., Cook, R., Wei, Y., Fang, Y., Hayes, D., Huang, M., Jain, A., Tian, H., 2017. Global patterns of drought recovery. Nature 548,

202–205. https://doi.org/10.1038/nature23021

Sippel, S., Reichstein, M., Ma, X., Mahecha, M.D., Lange, H., Flach, M., Frank, D., 2018. Drought, Heat, and the Carbon Cycle: a Review. Curr. Clim. Chang. Reports 4, 266–286. https://doi.org/10.1007/s40641-018-0103-4

Slette, I.J., Post, A.K., Awad, M., Even, T., Punzalan, A., Williams, S., Smith, M.D., Knapp, A.K., 2019. How ecologists define drought, and why we should do better. Glob. Chang. Biol. 25, 3193–3200. https://doi.org/10.1111/gcb.14747

Spohn, M., Bagchi, S., Biederman, L.A., Borer, E.T., Bråthen, K.A., Bugalho, M.N., Caldeira, M.C., Catford, J.A., Collins, S.L., Eisenhauer, N., Hagenah, N., Haider, S., Hautier, Y., Knops, J.M.H., Koerner, S.E., Laanisto, L., Lekberg, Y., Martina, J.P., Martinson, H., McCulley, R.L., Peri, P.L., Macek, P., Power, S.A., Risch, A.C., Roscher, C., Seabloom, E.W., Stevens, C., Veen, G.F. (Ciska., Virtanen, R., Yahdjian, L., 2023. The positive effect of plant diversity on soil carbon depends on climate. Nat. Commun. 14, 1–11. https://doi.org/10.1038/s41467-023-42340-0

Stocker, B.D., Zscheischler, J., Keenan, T.F., Prentice, I.C., Peñuelas, J., Seneviratne, S.I., 2018. Quantifying soil moisture impacts on light use efficiency across biomes. New Phytol. 218, 1430–1449. https://doi.org/10.1111/nph.15123

Sungmin, O., Bastos, A., Reichstein, M., Li, W., Denissen, J., Graefen, H., Orth, R., 2022. The Role of Climate and Vegetation in Regulating Drought-Heat Extremes. J. Clim. 35, 5677–5685. https://doi.org/10.1175/JCLI-D-21-0675.1

Sutton, C.D., 2005. Classification and Regression Trees, Bagging, and Boosting, Handbook of Statistics. Elsevier Masson SAS. https://doi.org/10.1016/S0169-7161(04)24011-1

Vicente-Serrano, S.M., Gouveia, C., Camarero, J.J., Beguería, S., Trigo, R., López-Moreno, J.I., Azorín-Molina, C., Pasho, E., Lorenzo-Lacruz, J., Revuelto, J., Morán-Tejeda, E., Sanchez-Lorenzo, A., 2013. Response of vegetation to drought time-scales across global land biomes. Proc. Natl. Acad. Sci. U. S. A. 110, 52–57. https://doi.org/10.1073/pnas.1207068110

Vicente-Serrano, S.M., Quiring, S.M., Peña-Gallardo, M., Yuan, S., Domínguez-Castro, F., 2020. A review of environmental droughts: Increased risk under global warming? Earth-Science Rev. 201, 102953. https://doi.org/10.1016/j.earscirev.2019.102953

Wang, Y., Zhou, H., Huang, J., Yu, J., Yuan, Y., 2023. A framework for identifying propagation from meteorological to ecological drought events. J. Hydrol. 625, 130142. https://doi.org/10.1016/j.jhydrol.2023.130142

Wei, X., He, W., Zhou, Y., Ju, W., Xiao, J., Li, X., Liu, Y., Xu, S., Bi, W., Zhang, X., Cheng, N., 2022. Global assessment of lagged and cumulative effects of drought on grassland gross primary production. Ecol. Indic. 136, 108646. https://doi.org/10.1016/j.ecolind.2022.108646

Wu, C., Zhong, L., Yeh, P.J.F., Gong, Z., Lv, W., Chen, B., Zhou, J., Li, J., Wang, S., 2023. An evaluation framework for quantifying vegetation loss and recovery in response to meteorological drought based on SPEI and NDVI. Sci. Total Environ. 906, 167632. https://doi.org/10.1016/j.scitotenv.2023.167632

Wu, J., Chen, X., Yao, H., Zhang, D., 2021. Multi-timescale assessment of propagation thresholds from meteorological to hydrological drought. Sci. Total Environ. 765, 144232. https://doi.org/10.1016/j.scitotenv.2020.144232

Xi, X., Yuan, X., 2023. Remote sensing of atmospheric and soil water stress on ecosystem carbon

and water use during flash droughts over eastern China. Sci. Total Environ. 868, 161715. https://doi.org/10.1016/j.scitotenv.2023.161715

Xu, S., Wang, Y., Liu, Y., Li, J., Qian, K., Yang, X., Ma, X., 2023. Evaluating the cumulative and time-lag effects of vegetation response to drought in Central Asia under changing environments. J. Hydrol. 627, 130455. https://doi.org/10.1016/j.jhydrol.2023.130455

Yuan, W., Zheng, Y., Piao, S., Ciais, P., Lombardozzi, D., Wang, Y., Ryu, Y., Chen, G., Dong, W., Hu, Z., Jain, A.K., Jiang, C., Kato, E., Li, S., Lienert, S., Liu, S., Nabel, J.E.M.S., Qin, Z., Quine, T., Sitch, S., Smith, W.K., Wang, F., Wu, C., Xiao, Z., Yang, S., 2019. Increased atmospheric vapor pressure deficit reduces global vegetation growth. Sci. Adv. 5, 1–13. https://doi.org/10.1126/sciadv.aax1396

Yuan, X., Wang, Y., Ji, P., Wu, P., Sheffield, J., Otkin, J.A., 2023. A global transition to flash droughts under climate change. Science (80-.). 380. https://doi.org/10.1126/science.abn6301

Zhang, X., Hao, Z., Singh, V.P., Zhang, Y., Feng, S., Xu, Y., Hao, F., 2022. Drought propagation under global warming: Characteristics, approaches, processes, and controlling factors. Sci. Total Environ. 838, 156021. https://doi.org/10.1016/j.scitotenv.2022.156021

Zhang, Yu, Zhang, Yangjian, Lian, X., Zheng, Z., Zhao, G., Zhang, T., Xu, M., Huang, K., Chen, N., Li, J., Piao, S., 2023. Enhanced dominance of soil moisture stress on vegetation growth in Eurasian drylands. Natl. Sci. Rev. 10. https://doi.org/10.1093/nsr/nwad108

Zhao, A., Yu, Q., Feng, L., Zhang, A., Pei, T., 2020. Evaluating the cumulative and time-lag effects of drought on grassland vegetation: A case study in the Chinese Loess Plateau. J. Environ. Manage. 261, 110214. https://doi.org/10.1016/j.jenvman.2020.110214

683 Zomer, R.J., Xu, J., Trabucco, A., 2022. Version 3 of the Global Aridity Index and Potential
684 Evapotranspiration Database. Sci. Data 9, 1–15. https://doi.org/10.1038/s41597-022-01493-1

685 **Figures**

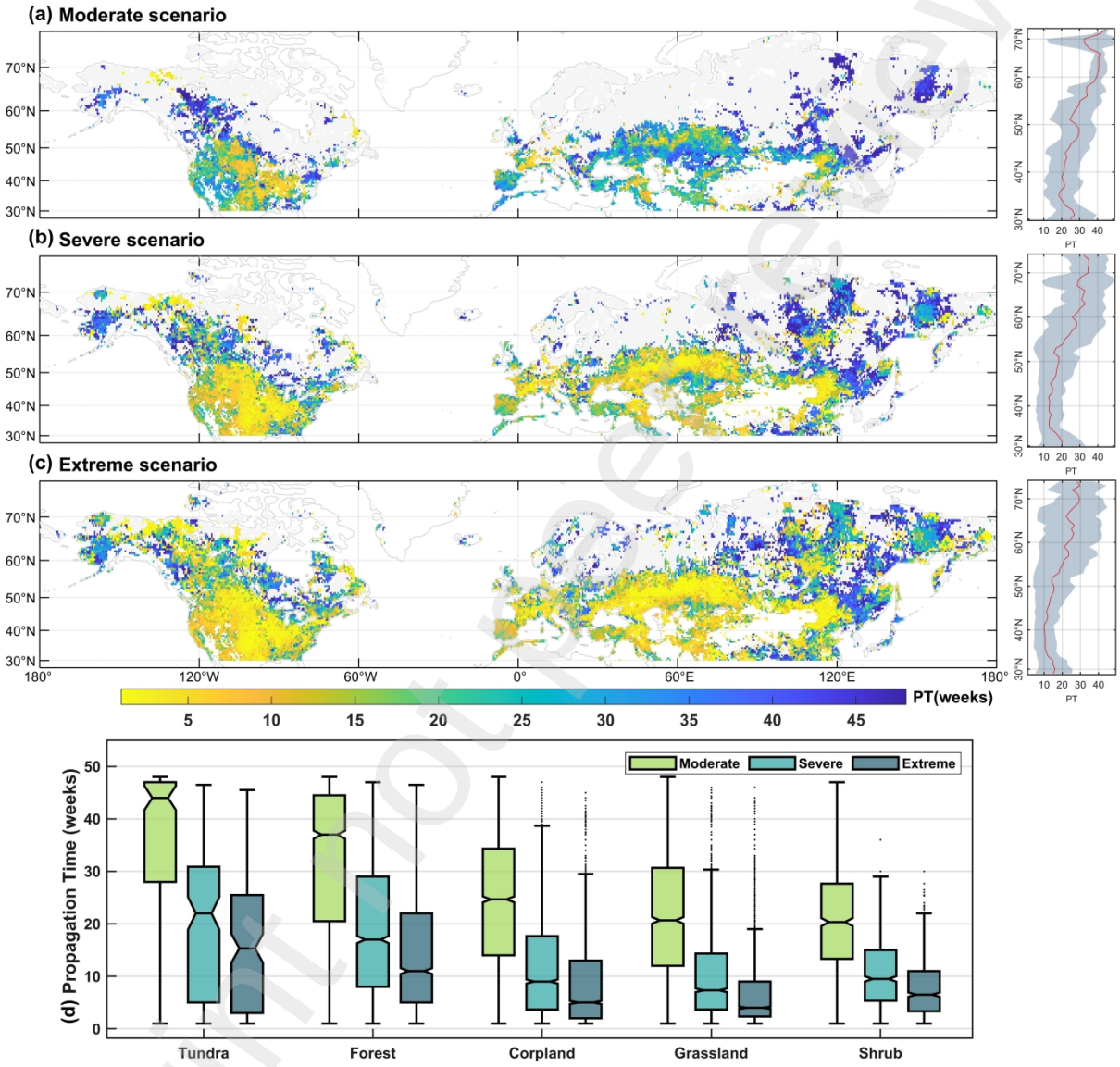

686

687 **Figure. 1 Spatial distribution of drought propagation time (PT) under different levels of meteorological**
688 **drought. (a)**, **(b)**, and **(c)** represent the spatial distribution of PT under moderate (-1.5<SPEI≤-1.0), severe (-
689 2<SPEI≤-1.5), and extreme (SPEI≤-2.0) drought scenarios. The red curve on the right side of the map represents
690 the average spatial distribution of PT along different latitudes, and the shaded band represents the interquartile range

of the mean PT. The gray areas on the map represent regions where vegetation cover exists but exhibits a negative correlation coefficient with SPEI in the long-term growth status (see Methods). This implies that vegetation in these areas is in an energy-controlled state. Therefore, these regions were not included in this study. **(d)** is the boxplots of PT of different vegetation types (i.e., tundra, forest, cropland, grassland, and shrub) under the three drought scenarios. The upper and lower edges of the box represent the 75th and 25th percentiles, respectively, and the middle line represents the median PT. Points outside the box indicate outliers.

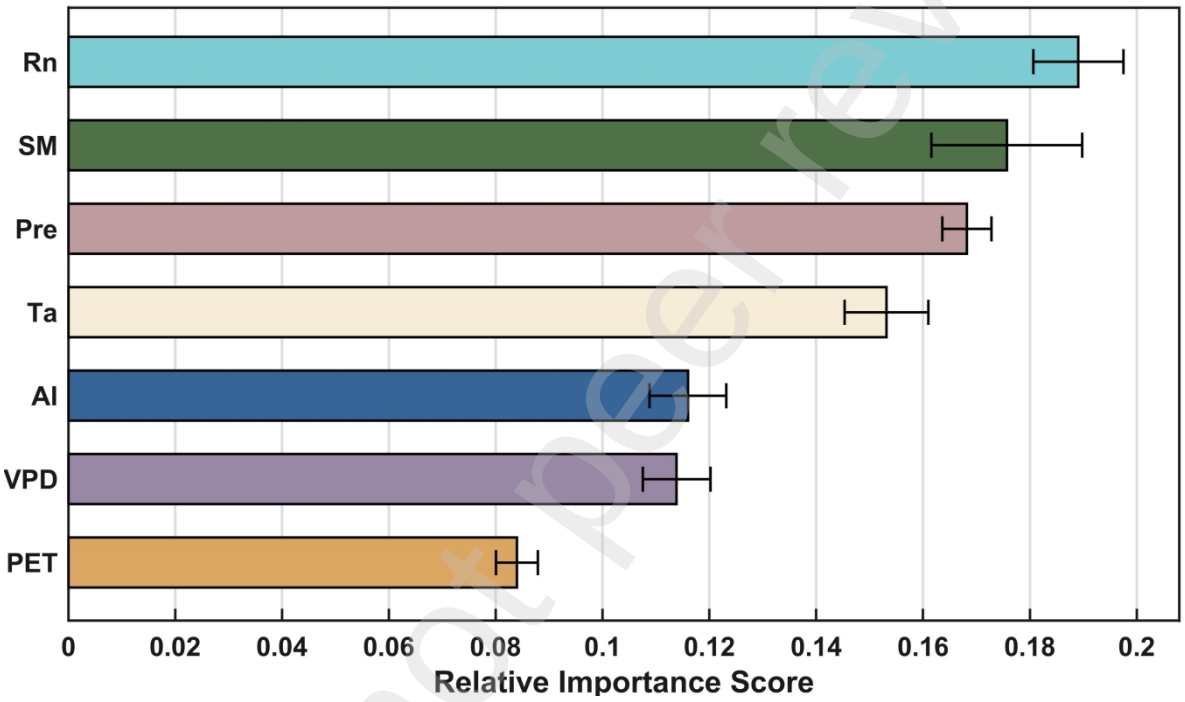

Figure. 2 Relative importance scores ranking of different variables in influencing the spatial distribution magnitude of drought propagation time (PT) based on the Random Forest model. The error bars in the figure represent a 95% confidence interval.

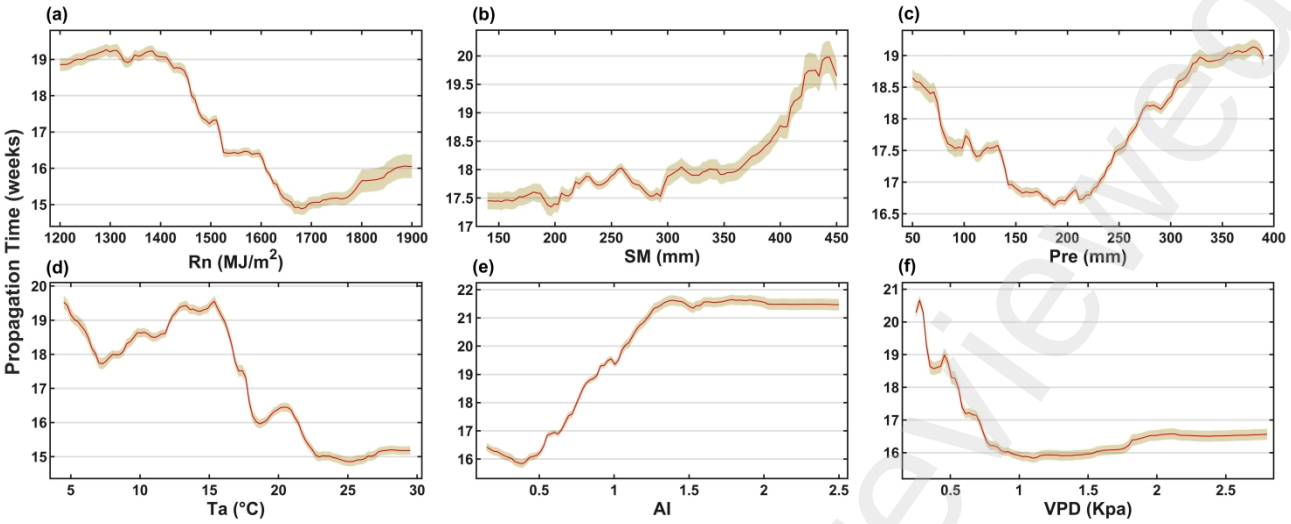

Figure. 3 Response functions of different variables that influence the spatial distribution of drought PT. (a)-(f) represent the independent response processes of PT to solar radiation (Rn), soil moisture (SM), precipitation (Pre), air temperature (Tm), aridity index (AI), and vapor pressure deficit (VPD). **(a)-(f)** are ranked in descending order according to the relative importance scores of the influencing variables (as shown in Supplementary Fig. 2), with the y-axis representing drought PT and the x-axis representing the variation range of each influential variable during summer. The red solid line in the figure represents the results calculated using all grids data for each variable, while the shaded band represents the 95% confidence interval obtained through bootstrap sampling method (see **Methods**).

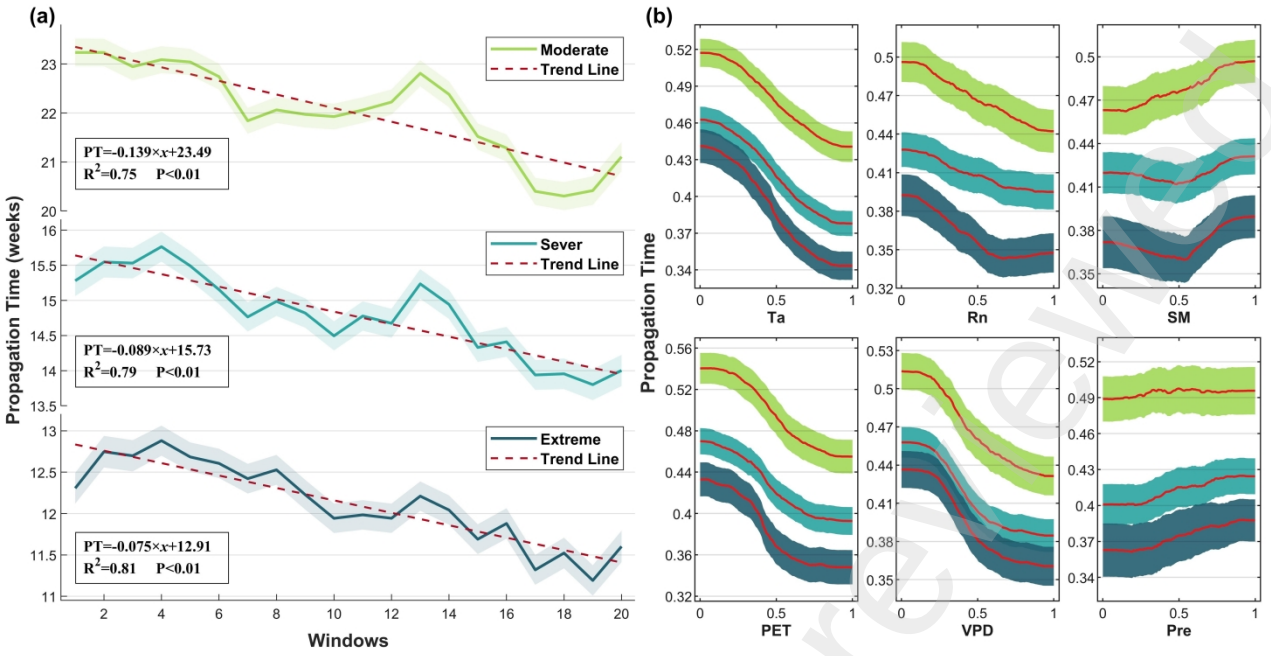

Figure. 4 The overall average trend of drought PT in the NHE over the last three decades and the response functions of the dominant variables driving the changes of PT. (a) The lines in the figure, from top to bottom, represent the average trends of PT under moderate, severe and extreme drought scenarios. The shading denotes the mean PT uncertainties at a 95% confidence interval. The red dashed line represents the fitted trend line obtained from the data of each window. Below the line are the linear trend equation, coefficient of determination (R^2), and the significance level of the trend. **(b)** Response functions of the dominant variables driving changes in PT. The y and x-axes represent PT and the range of variation for each driving variable, respectively. To facilitate comparison between grid cells, we normalized both PT and its driving factors. The red curve represents the average response function of all grid cells, and the shaded band around the curve represents the 95% confidence interval based on the bootstrap sampling method. The colors of the shaded bands ranging from light to dark correspond to moderate, severe, and extreme drought scenarios, respectively.

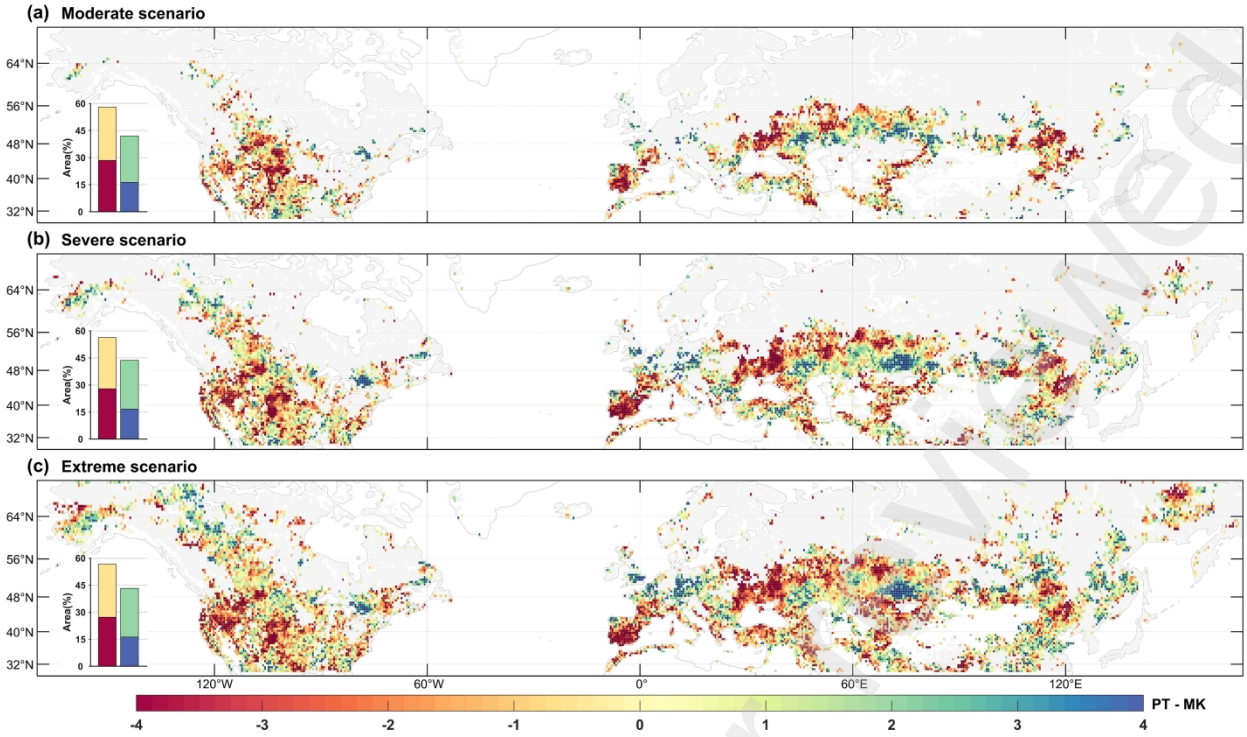

Figure. 5 Dynamic changes of drought PT during summer in the NHE over the last three decades (1982-2015). (a), (**b**), and **(c)** represent the trends of PT under moderate, severe, and extreme meteorological drought scenarios, respectively, obtained using the MK trend test. The colors ranging from red to blue indicate the shortening and increasing trends of PT, respectively. The grid points on the map represent the trends that have passed the significance test with $P<0.01$. The bar chart illustrates the area proportion of different trends, with the first bar indicating the percentage of areas with a significant and non-significant shortening trend in PT, represented by deep red and light yellow, respectively. The second bar represents the percentage of areas with a significant and non-significant increase trend in PT, shown by deep blue and light green, respectively.

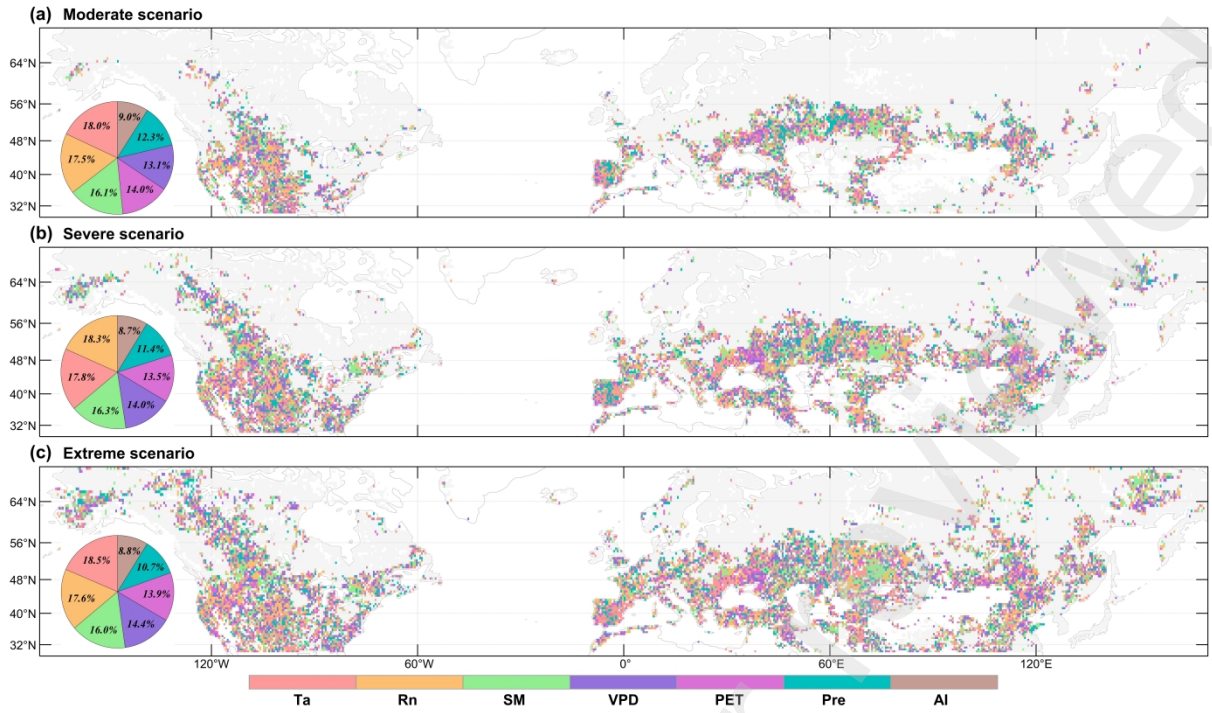

Figure. 6 Spatial distribution of the dominant driving variables influencing changes in drought PT. (a), **(b)**, and **(c)** represent the dominant driving variables affecting PT changes in moderate, severe, and extreme meteorological drought scenarios, respectively, based on the Random Forest model (see **Methods**). Different colors represent different driving factors, and the pie charts indicate the relative proportion of the influence area of each variable.

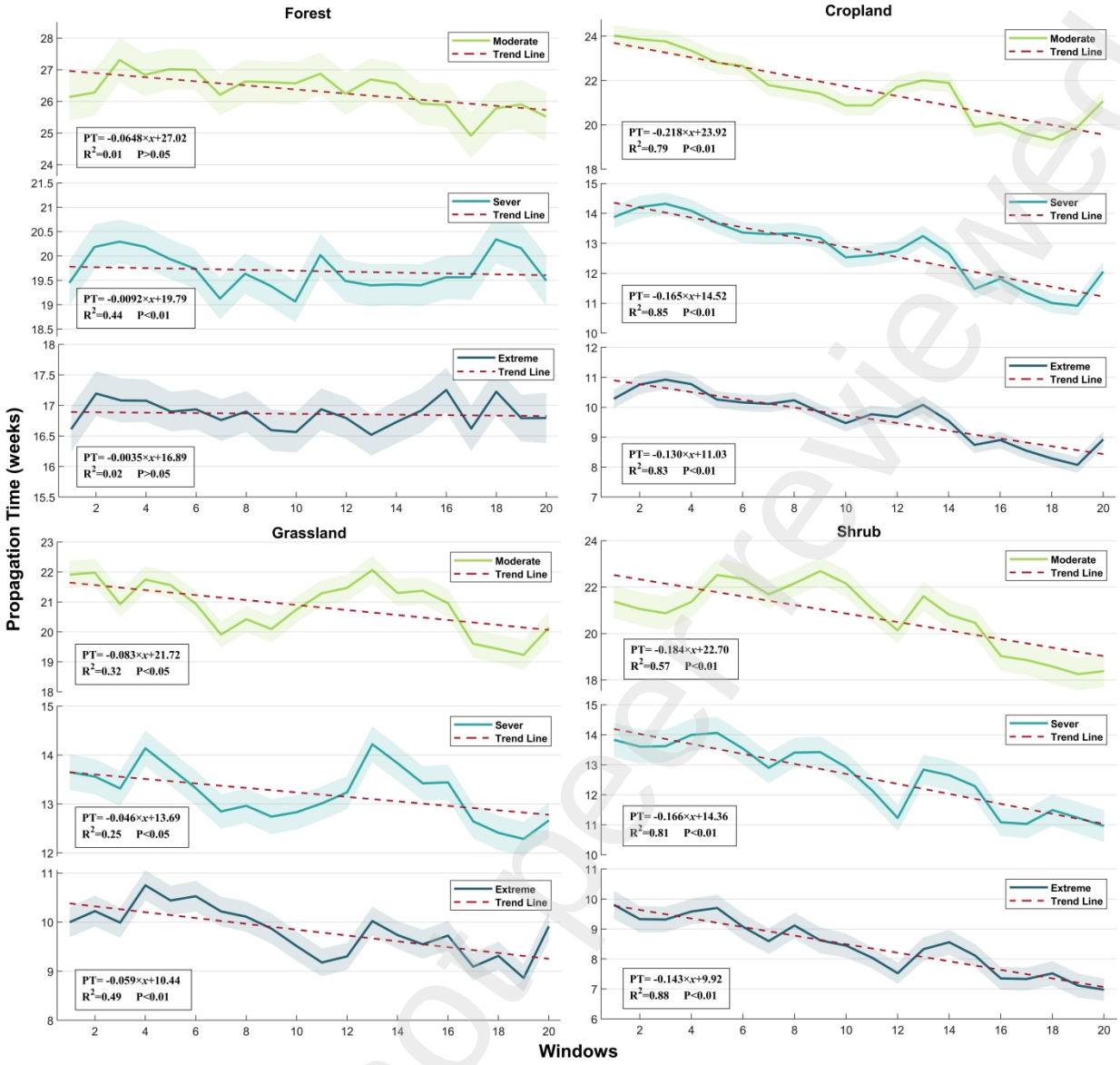

743

744 **Figure. 7 The average trends in drought PT for different vegetation types in the NHE over the last three**

745 **decades.** The light green, light blue, and dark blue lines in the graph represent the variations of PT under moderate,

746 severe, and extreme meteorological drought scenarios, respectively. The shading denotes the mean PT uncertainties

747 at a 95% confidence interval. Below the line are the fitted linear trend equation, coefficient of determination (R^2),

748 and the significance level of the trend.

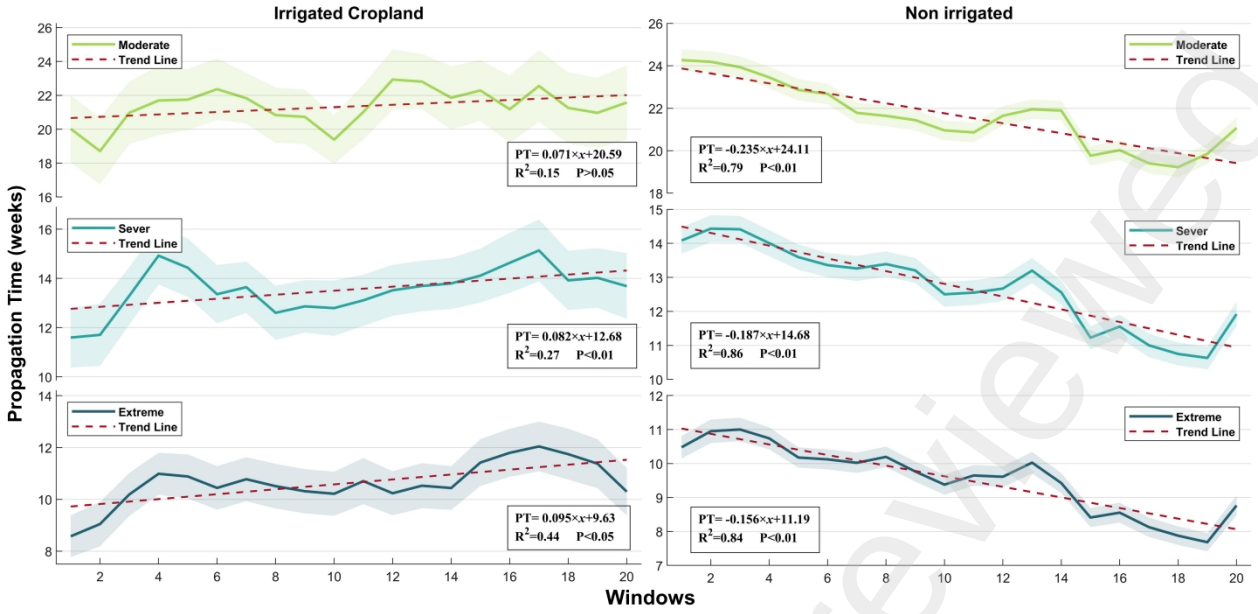

749

750 **Figure. 8 A comparison of the average trends in drought PT between irrigated and non-irrigated agricultural**

751 **fields in the NHE over the last three decades.** The light green, light blue, and dark blue lines in the graph represent

752 the variations of PT under moderate, severe, and extreme meteorological drought scenarios, respectively. The

753 shading denotes the mean PT uncertainties at a 95% confidence interval. Below the line are the fitted linear trend

754 equation, coefficient of determination (R^2), and the significance level of the trend.